Optimization of electrode of a right-angled electromagnetic flowmeter using CFD simulation

Weijie Chen[1,2], Haohao Xu[1], Chengxu Tu[2], Xianfeng Li[2], Wenkun Gao[3], Jianli Zhang[3], Xiang Li[1], Fubing Bao[2,*]

[1]Zhejiang Energy Technology Research Institute Co. Ltd, Hangzhou 310018, Hangzhou, China;
[2]Zhejiang Provincial Key Laboratory of Flow Measurement Technology, College of Metrology and Measurement Engineering, China Jiliang University, Hangzhou, China
[3]Shanghai Tianshi Measurement & Control Equipment Co., Ltd, Shanghai, China
E-mail (Fubing Bao): dingobao@cjlu.edu.cn

Abstract

Currently, electromagnetic flowmeters must typically be inserted into a straight pipe, which usually requires a larger installation space. To improve installation adaptability, a novel right-angled electromagnetic flowmeter is proposed. As the measurement signal of the electromagnetic flowmeter is closely related to the flow state of its internal fluid, a large-eddy simulation (LES) was used to study the influence of the shape of the electrode and the contraction section of the flowmeter on the flow characteristics inside the flowmeter to reveal the relationship between them along with the measurement accuracy. A comparison between the numerical results and the experimental results was also performed. The velocity fluctuations of the monitoring points around the cone and flat electrodes were compared, and it was found that the overall measurement error of the cone electrodes was smaller than that of the flat electrodes. The experimental results showed that the pulsation of the voltage signal measured from the cone electrode is smaller than that of the flat electrode. In addition, the absolute value of the error in the small flowrate is much smaller than that of the flat electrode. Consequently, the measurement performance of the cone electrode is better. In addition, the largest velocity fluctuation occurred between the electrode wall and tube wall, indicating that installing the coil should avoid exciting strong magnetic fields here.

1. Introduction

Electromagnetic flowmeters are an important flow measurement tool widely used in everyday urban environments. They can be used to measure the instantaneous and cumulative flows of conductive liquids, and are thus widely used in chemical, petroleum, steel, metallurgical, and other industries. Since their invention, the measurement accuracy of electromagnetic flowmeters has been significantly improved. Starting with insertion flowmeters, different types of electromagnetic flowmeters have since been developed to meet various needs, ranging from monoblock flowmeters to two-wire, then explosion-proof, and now high-pressure electromagnetic flowmeters have become the most widespread and universally applicable flowmeters [1]. The future of electromagnetic flowmeters will focus on changing their structure to adapt to the increasingly complex measurement environment and to meet individual measurement needs.

For electromagnetic flowmeter performance optimisation, researchers are currently using theoretical analysis, numerical simulation, and experimental studies to carry out systematic research on the electrode shape [2-4], contraction structure [12], coil shape [9], magnetic circuit structure, and other aspects of electromagnetic flowmeters.

The electrode, as the flow signal acquisition end of the electromagnetic flowmeter, is the key to optimising the performance of the electromagnetic flowmeter. Asali et al. [2] first designed a ring electrode, based on which Fossa et al. [3] demonstrated that the ring electrode has a higher resolution than the parallel plate electrode for water holding rate measurement. Jin et al. [4] used the finite element method (FEM) to optimise geometric parameters of an array of eight ring electrode conductivity probes, and Zhai et al. [5] developed an array of four ring electrode conductivity probes based on this approach to improve the flow detection accuracy of electromagnetic flowmeters.

The effect of the electromagnetic flowmeter contraction structure on the flow field in the measurement section is also an important factor in its performance improvement. Heijnsdijk et al. [6] used a contraction section as part of the electromagnetic flowmeter pipe structure and designed intermediate pipe sections with different shapes. Korsunskii [7] et al. demonstrated that, for rectangular section pipes, the induced signal on the electrode does not depend on the flow velocity distribution. Lim [8] improved the traditional electromagnetic flowmeter by designing rectangular pipe and magnetic field structures and analysing the weight function distribution of the rectangular electrodes.

In addition, the potential application of coil shape and magnetic circuit structure to enhance the performance of electromagnetic flowmeters has also received extensive attention. Kanai et al. [9] compared the effect of three coil shapes on the relative sensitivity of electromagnetic blood flowmeters through theoretical analysis and experimental studies, finding that saddle-shaped coils corresponded to better measurement performance of electromagnetic flowmeters. Christensen et al. [10] developed a finite element simulation model of an electromagnetic flowmeter and compared the magnetic field distribution inside the electromagnetic flowmeter with two magnetic circuits, the quadrupole sheet model, and the diamond-coil model. The finite element simulation results of the magnetic field were experimentally verified, suggesting that the sensitivity of the diamond-coil model is less affected by the magnetic circuit under the same circumstances. Liu et al. [11] compared the sensitivity of different pipe design solutions by analysing the magnetic circuit of a uniform circular tube, a partially constricted circular tube, and a partially constricted rectangular tube electromagnetic flow sensor. The results suggested that using a partially constricted rectangular tube form could effectively improve the magnetic circuit efficiency and transducer sensitivity.

As mentioned above, most domestic and international research has focused on the impact of the internal structure of conventional electromagnetic flowmeters on measurement performance, while little research has focussed on the impact of insertion type flowmeters on measurement performance. Therefore, this study proposes an insertion type right-angled electromagnetic flowmeter, whose 90° curved tube insertion structure is suitable for online installation and disassembly in industrial sites, to meet the urgent need for flow measurement in industrial sites with limited installation space. In addition, this study investigates the influence of flat and cone electrodes and the shape of the contraction section on the measurement performance of the electromagnetic flowmeter and optimises its internal structure.

2. Model descriptions

2.1 Physical model

The inlet pipe of the proposed insertion type right-angled electromagnetic flowmeter is perpendicular to the outlet. The specific structure is as shown in Figure 1, the inlet pipe diameter is 50mm, the diameter of the measuring pipe section is 16mm, the total length of the pipe is 300mm, and the diameter of the sensor is 6mm. The sensor has two axisymmetric electrodes of equal size, and the contraction section is located in the electrode upstream. Its measuring range is 0.5~10 m/s, and the working pressure is 10~42 MPa, indicating a kind of electromagnetic flowmeter with strong pressure resistance. The insertion right angle design is more suitable for restricted installation sites than the traditional structure.

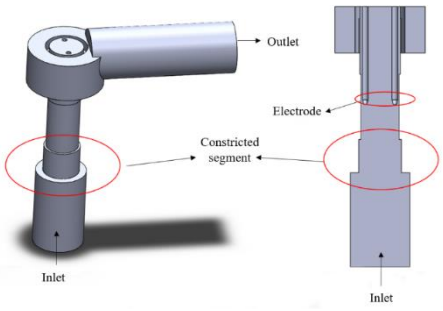

Figure 1: Structure of right-angled electromagnetic flowmeter.

2.2 CFD model

Conventional methods for numerical simulation of turbulence include DNS, RANS, and LES; LES (Large Eddy Simulation) is suitable for high precision numerical simulation of flow processes at high Reynolds numbers and for sufficiently saving computational resources required for the simulation needs of this study. The Large Eddy Model is a recent approach to turbulence research, where the N-S equations can be solved directly on a computer. The basic idea of the model is that the region of the flow is divided into a large-scale vortex motion part and a small-scale part. The flow properties of the large-scale vortex motion part can be obtained by solving the non-constant three-dimensional N-S equation, while the small-scale part of the flow can be obtained with a more general model and does not require direct computation.

The control equations for LES are obtained by filtering the N-S equations in three dimensions or physical space. For homogeneous turbulent states, convolution filters are commonly used to define the large-scale components of the variables, and the filtered variables are defined as follows.

$$\bar{\varphi}(x)=\int_D \varphi(x')G(x,x')dx' \tag{1}$$

where D is the flow region; x is the spatial coordinate; $G(x,x')$ is the filter function that determines the scale of the vortex being solved.

The filter function $G(x,x')$ corresponds to equation (1)

$$G(x,x')=\begin{cases}1/V(x), x\in v(x)\\ 0, x\notin v(x)\end{cases} \tag{2}$$

where x is the spatial coordinate; $V(x)$ is the control volume; $v(x)$ is the range of coordinates within the control body.

After filtering the incompressible N-S equation, the LES control equation can be obtained as follows:

$$\frac{\partial \rho}{\partial t} + \nabla \bullet \left(\rho \bar{u}\right) = 0 \qquad (3)$$

$$\frac{\partial \left(\rho \bar{u}\right)}{\partial t} + \nabla \bullet \left(\rho \bar{u}_i \bar{u}\right) = \frac{\partial \bar{\rho}}{\partial i} + \nabla \bullet \left(\mu \nabla \bar{u}_i\right) - \nabla \tau_{ij} \qquad (4)$$

where i, j take x, y, z; τ_{ij} is the subgrid stress, $\tau_{ij} = \rho \overline{u_i u_j} - \rho \bar{u}_i \bar{u}_j$.

According to the actual dimensions, the fluid domain model is constructed, while the ICEM software is used to mesh the fluid domain model of the electromagnetic flowmeter. Focus on the flow characteristics of the flow field near the electrode of the electromagnetic flowmeter, the grids of electrode structure need to take local encryption measures, and part of the grids are shown in Figure 2. According to the grid-independent verification, when the number of grids of the inlet and outlet is greater than or equal to 3.12 million, the pressure does not change significantly with the increase in the number of grids; thus, 3.12 million should be chosen for grid number calculation. Considering that the fluid in the pipe cannot be fully developed by giving the model an inlet velocity directly, a fully developed velocity inlet is given directly at the inlet to reduce the computational effort.

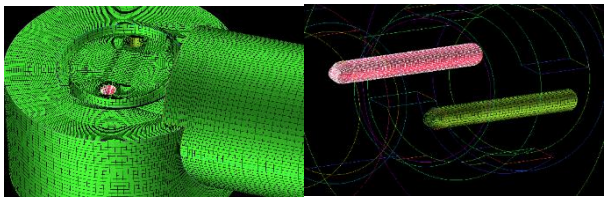

Figure 2: Schematic diagram of part of the structural grid

3. Electromagnetic flowmeter structure analysis and optimisation

According to the operating range of the electromagnetic flowmeter, this paper selects a velocity inlet of 3m/s, a pressure outlet of 10MPa, an internal fluid medium of water, a reference pressure of one atmosphere, and a temperature setting of 20°C as the working conditions of this model in the simulation software.

To ensure the original model electrode length remains unchanged, the contact radius between the tip of the electromagnetic flowmeter and the fluid was reduced from 1.5 mm in the original model to 1 mm and 0.5 mm, respectively; the smaller the contact area between the tip of the electrode and the fluid, the more stable the flow field near the electrode after comparison. Considering the process and the service life of the electrode, an electrode with a 1mm radius of the tip plane was used. The optimized electrodes are shown in Figure 3, and the processed electrodes are shown in Figure 4.

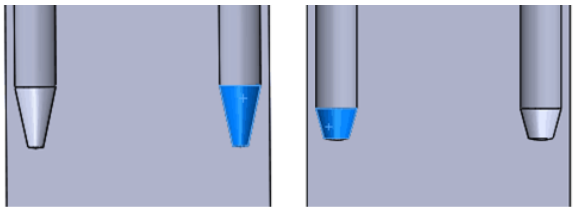

(a) Cone (b)Flat

Figure 3: Electrode optimisation.

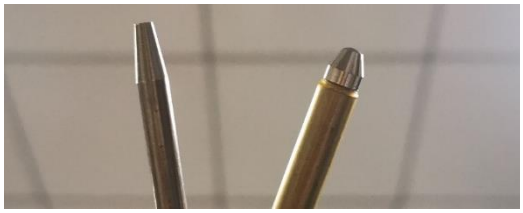

Figure 4: Physical view of electrodes.

In this study, 46 monitoring points were selected in the vicinity of the electrode, including the electrode axis and radial plane detection points. Considering the downstream of the electrode as the positive direction, the distance between the monitoring point (plane) and the top of the electrode is expressed as the measuring distance D. The monitoring point is located on the electrode axis, while the detection plane is orthogonal to the direction of the electrode axis. $D = -1$ means that the monitoring point (plane) is located upstream of the electrode and 1 mm from the electrode tip plane; $D = 0$ means that the monitoring point (plane) is in the plane where the electrode tip is located; $D = 1$ means that the monitoring point (plane) is located. The distribution of the monitoring points in the direction of the electrode axis is shown in Figure 5(a), with monitoring points located at $D = -1, -2, -3, -4$, and -5. The monitoring points on the radial plane of the electrode are shown in Fig. 5(b), with the detection planes located at $D = -2, -1, -0.5, 0$, and 1. Eight monitoring points are set up on the monitoring planes of $D = 0$ at the top of the electrode and $D = 1$ downstream of the electrode, located on the inner and outer rings 2 mm and 2.5 mm away from the electrode axis, respectively. The phase difference of each monitoring point is 90°, the positions of the monitoring points on the inner and outer rings correspond, and the distribution of the monitoring points is shown in the upper left part of Fig. 5(b). Nine monitoring points are set up in the detection planes of $D = -0.5, -1$, and -2 upstream of the electrode. The positions of the monitoring points of the inner and outer rings are the same as above, but the ninth monitoring point is located on the electrode axis; the monitoring points are shown in the upper right diagram of Fig. 5(b).

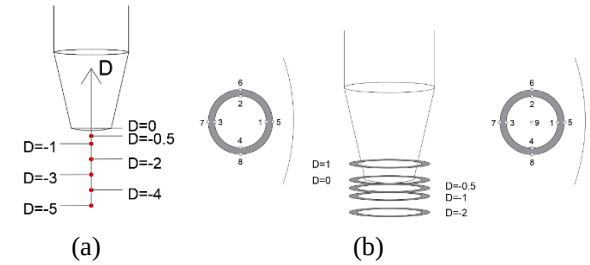

Figure 5: Monitoring points around electrodes

According to the comparison of the error bars of the monitoring points on the electrode axis in Figure 6, the velocity near the cone electrode is greater than the flat one and that the error bars are smaller when the monitoring points are closer to the electrode. The velocity error of the flat electrode is about 17% at the closest point to the electrode, while the error of the cone electrode is less than 2%.

The velocity magnitudes and their errors at various points on the monitoring surface 2mm and 1mm upstream of the electrode are shown in Figures 7 and 8, respectively. For monitoring points located further upstream of the electrode, the velocity distribution around the cone electrode is more uniform than that of the flat electrode for the same location.

The velocity magnitudes and their errors at various points on the monitoring surface 0.5mm upstream of the electrode are shown in Figure 9. The velocity distribution at various points on both the cone and flat electrodes here is irregular, indicating that the fluid here is obstructed by the electrode plane when it flows through it. The velocity monitoring value at the centre point is greater than that of the flat electrode because the plane of the cone electrode is smaller and there is less reflux.

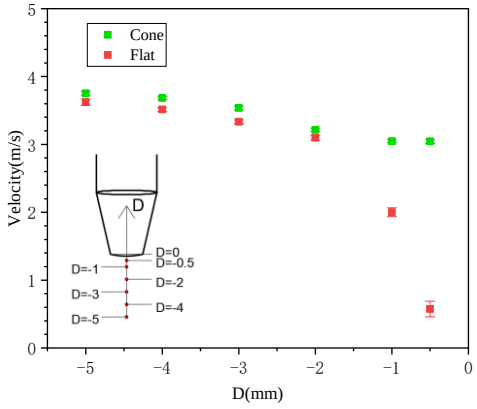

Figure 6: Comparison of error bars for points monitored on the electrode axis.

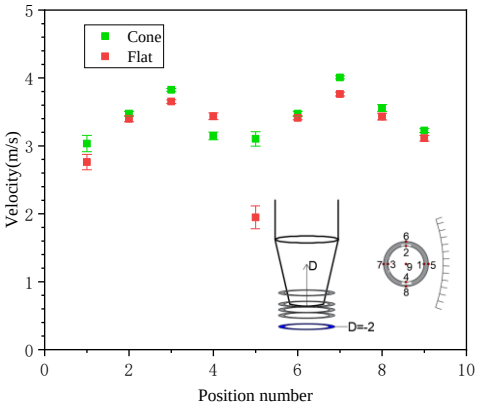

Figure 7: Comparison of error bars for monitoring points in the D=-2mm plane upstream of the electrode apex.

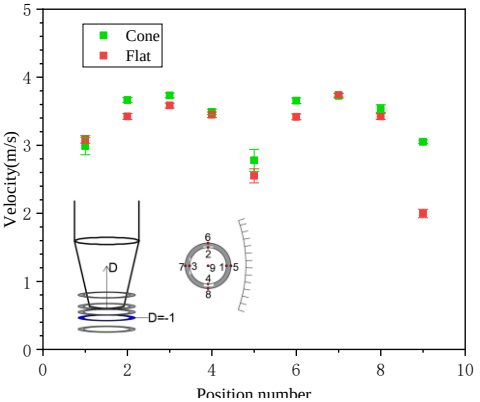

Figure 8: Comparison of error bars for monitoring points in the D=-1mm plane upstream of the electrode apex.

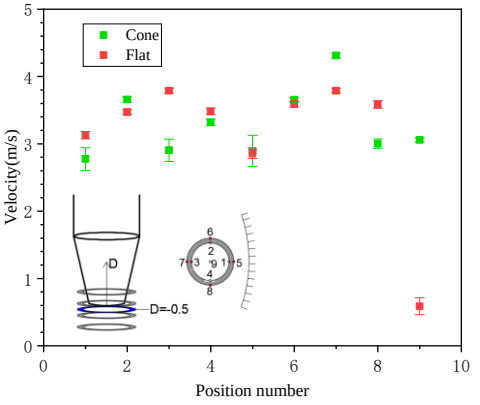

Figure 9: Comparison of error bars for monitoring points in the D=-0.5 mm plane upstream of the electrode apex.

The velocity distribution of the points on the detection surface at the electrode plane and their errors are shown in Figure 10. The velocity of the tip at the monitoring point between the electrode wall and the measurement tube wall (monitoring points 1 and 5) is smaller and the error is larger, while the velocities of the other points are greater than those of the flat electrode and the error is smaller than that of the flat electrode.

According to Figure 11, when the monitoring surface is located downstream of the electrode, the velocity distribution of the monitoring points is similar to that at the electrode plane, the cone electrode is more influenced by the wall, the monitoring points between the electrode wall and the measuring tube wall (monitoring points 1 and 5) have smaller velocities and larger errors, and the velocities at all other points are larger than the flat electrode and the errors are smaller than the flat electrode.

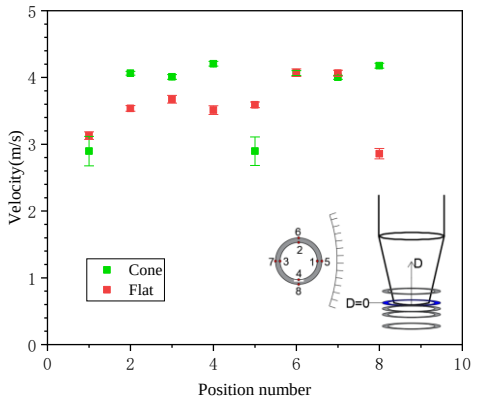

Figure 10: Comparison of error bars for monitoring points in the plane where the electrode vertices are located.

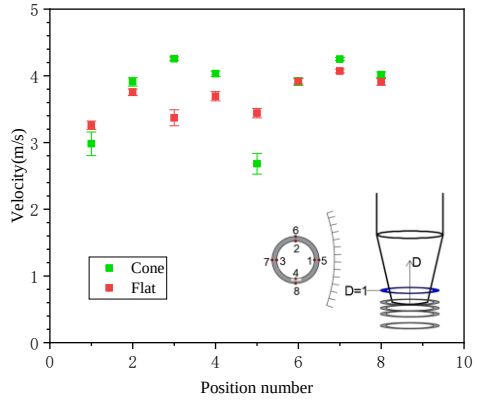

Figure 11: Comparison of error bars for points at monitoring points D=1mm downstream of the electrode apex.

In general, the velocities of the monitoring points around the cone electrodes are less than those of the flat electrodes. Individual errors at points between the electrode and the wall can be significant. Based on the above results, the following conclusions can be drawn：

1. Velocity fluctuations at the monitoring point between the electrode wall and the measuring tube wall are large and should be avoided as far as possible when installing the magnetic circuit system, taking into account the area covered by the coil, to avoid them having an impact on the accuracy of the measured value.
2. The tip electrode has a small impact on the flow in the measured tube of the flowmeter, the velocity measurement error is small, and the optimization is conducive to improving the electromagnetic flowmeter measurement performance.

4. Experimental validation of electrode optimisation

According to the above flow field analysis of the electrode shape optimisation of the electromagnetic flowmeter, this section presents the experimental tests on the overall effect of the electrode shape optimisation on the electromagnetic flowmeter before and after measuring the voltage signal output from the flat and cone electrode electromagnetic flowmeter and the actual flow rate at different flow points.

Figure 12: Diagram of the experimental verification set-up for electrode optimisation of electromagnetic flow meters.

The experimental device comprises a water tank, water pump, pressure stabilization device, tested flowmeter, standard flowmeter, and standard container. The device diagram is shown in Figure 12. The device uses the pump to pump water from the tank through the pressure regulator to obtain the pressure environment required for the experimental measurement. The water then flows through the tested flowmeter to be measured, then into the standard flowmeter, further into the split standard flowmeter to measure the standard flow rate, and finally into the standard container. The flowmeter is connected to a computer, and the voltage signal from the electromagnetic flowmeter is read when a steady flow of fluid is passed through it after one stage of amplification. The flow rate value of the two electromagnetic flowmeters was recorded, with several repeated measurements made. We then calculated the error and took the average value; part of the experimental data as shown in Tables 1 and 2.

Table 1: Measurement data for flat electrodes.

Standard flow (m^3/h)	Measured flow (m3/h)	Standard volume (L)	Measured volume (L)	Error (L)	Error mean (%)	Rep (%)
13.9	13.875	115.452	115.796	0.297	0.274	0.026
	13.876	112.098	112.409	0.278		
	13.880	114.050	114.331	0.246		
8.6	8.650	142.789	144.242	1.018	1.036	0.018

	8.647	142.138	143.636	1.054		
	8.649	142.388	143.862	1.035		
4.4	4.404	23.701	24.960	5.310	5.420	0.098
	4.407	23.792	25.089	5.453		
	4.405	23.782	25.089	5.497		

Table 2: Measurement data for cone electrodes.

Standard flow (m^3/h)	Measured flow (m3/h)	Standard volume (L)	Measured volume (L)	Error (L)	Error mean (%)	Rep (%)
14.3	14.272	117.448	117.323	-0.106	-0.183	0.045
	14.275	117.048	116.825	-0.190		
	14.266	117.348	117.210	-0.118		
6.9	6.951	57.172	57.227	0.095	-0.014	0.099
	6.950	56.021	55.965	-0.099		
	6.949	57.222	57.200	-0.039		
3.3	3.263	53.568	54.410	1.573	1.559	0.031
	3.260	54.319	55.177	1.580		
	3.262	53.468	54.282	1.523		

By comparing the two electrodes collected in the computer after a level of amplification of the electrical signal can be seen, the flat electrode voltage signal pulsation amplitude is larger, and the peak values of each cycle amplitude pulsation are different. Furthermore, the cone electrode voltage signal pulsation amplitude is smaller, and the amplitude of each cycle will be close to a fixed value. For the same type of electromagnetic flowmeter, considering the electromagnetic flowmeter induction electric potential change, speed, size, and magnetic field strength have a relationship, only changing the shape of the electrode does not change the magnetic circuit system or the magnetic field strength. The voltage signal is affected by the velocity distribution of electromagnetic flowmeter. Considering this can be seen, for the insertion of right-angle bend electromagnetic flowmeter, cone electrode is more conducive to signal stability than the flat electrode.

5. Conclusion

This study proposes an insertion type right-angled electromagnetic flowmeter, which can be applied to industrial sites with restricted installation sites and can work in high pressure environments, unlike traditional electromagnetic flowmeters. Through electrode shape optimization, experiments, and numerical analysis, it was found that the error between monitoring points of the flat electrode and the cone electrode was large. However, the results of the cone electrode near the monitoring point of the velocity fluctuations were smaller than the flat electrode, and the velocity error is also less than the flat electrode in all other monitoring points. The cone electrode voltage signal pulsation in multiple cycles always tends to a stable value, while the voltage signal pulsation of the cone electrode always tends to a stable value in several cycles, while the flat electrode shows irregular pulsation in each cycle.

6. Acknowledgements

This work was supported by the Key R &D Plan Project of Zhejiang Province (2021C01099) and the Fundamental Re-search Funds for the Provincial Universities of Zhejiang (2020YW06, 2020YW19). Authors would acknowledge Zou, Wang, Zhuo in M4 Group for processing the experimental data.

References

[1] CAI, *Electromagnetic flow meters* (Beijing, CHINA PETROCHEMICAL PRESS), 2004.

[2] J. C. Asali, T. J. Hanratty, and P. Andreussi, “Interfacial drag and film height for vertical annular flow”, *AIChE J*, Vol.31, no. 6, pp. 895–902, Jun. 1985.

[3] M. Fossa, “Design and performance of a conductance probe for measuring the liquid fraction in two-phase gas-liquid flows”, *Flow Meas. Instrum*, Vol. 9, no. 2, pp. 103–109, Jun. 1998.

[4] N. D. Jin, Z. Xin, J. Wang, Z. Y. Wang, X. H. Jia, and W. P. Chen, “Design and geometry optimization of a conductivity probe with a vertical multiple electrode array for measuring volume fraction and axial velocity of two-phase flow”, *Meas. Sci. Technol*, Vol. 19, no. 4, p. 045403, Apr. 2008.

[5] L. Zhai, N. Jin, and Y. Zong, “The development of a conductance method for measuring liquid holdup in horizontal oil-water two-phase flows”, *Meas. Sci. Technol.*, Vol.23, no. 2, pp.344-347, Feb. 2012

[6] Heijnsdijk A M, Willigen A L, Lodege G R,“Magneto inductive flowmeter and method for producing a magnetinductive flowmeter”: US, 7, 261, 001 B2 [P]. (2007-08-28) [2012-05-26].

[7] Korsunskii L, “Electromagnetic flowmeter with a rectangular channel”, *Measurement Flowmeter*, 1960, 3(10): 893-899

[8] Lim S, The improvement of meter performance of EM sensing flowmeters using software modeling [D]. England: Cranfield University, 2008.

[9] Kanai H, “The effects upon electromagnetic flowmeter sensitivity of non-uniform fields and velocity profiles”, Medical and biological engineering, 7(6):661-676, 1969.

[10] Christensen T A, Willatzen M, “Investigating the effect of magnetic pipes connected to electromagnetic flowmeters using experimentally validated finite element models”, Flow Measurement & Instrumentation, 21(1):62-69,2010.

[11] Liu T, Zhang G, “Magnetic Circuit Design for Elecromagnetic flow Transducer with Locally Shrunk Measurement Pipe”, *International Conference on Future Computer and Communication Engineering*. (Atlantis Press), 11-14, 2014.